Design, Biological Evaluation and Molecular Modelling of Tetrahydroisoquinoline Derivatives: Discovery of A Potent P-glycoprotein Ligand Overcoming Multi-Drug Resistance in Cancer Stem Cells.

Chiara Riganti,[] Marialessandra Contino,[§] Stefano Guglielmo,*[‖] Maria G. Perrone,[§] Iris C. Salaroglio,[] Vladan Milosevic,[] Roberta Giampietro,[§] Francesco Leonetti,[§] Barbara Rolando,[‖] Loretta Lazzarato,[‖] Nicola A. Colabufo,[§,#] and Roberta Fruttero.[‖]*

[]Dipartimento di Oncologia, Università degli Studi di Torino, via Santena 5/bis, 10126, Torino, Italy

[§]Dipartimento di Farmacia-Scienze del Farmaco, Università degli Studi di Bari ALDO MORO, via Orabona 4, 70125, Bari Italy

[‖]Dipartimento di Scienza e Tecnologia del Farmaco, Università degli Studi di Torino, Via P. Giuria 9, 10125 Torino, Italy

[#]Biofordrug s.r.l., Spin-off dell'Università degli Studi di Bari ALDO MORO, Via Orabona 4, 70125 Bari, Italy

KEYWORDS Multi-drug resistance, P-glycoprotein, cancer stem cells, drug design, molecular modelling.

ABSTRACT P-glycoprotein (P-gp) is a well-known membrane transporter responsible for the efflux of an ample spectrum of anticancer drugs. Its relevance in the management of cancer chemotherapy is increased in view of its high expression in cancer stem cells (CSCs), a population of cancer cells with strong tumour-promoting ability. In the present study, a series of compounds were synthesized through structure modulation of **MC70** ([4'-(6,7-dimethoxy-3,4-dihydro-1H-isoquinolin-2-ylmethyl)biphenyl-4-ol]), modifying the phenolic group of the lead compound. Among them compound **5b** emerged for its activity against the transporter (EC_{50} = 15 nM) and was capable of restoring Doxorubicin anti-proliferative activity at non-toxic concentration. Its behaviour was rationalized through a molecular modelling study consisting of a well-tempered metadynamics simulation, that allowed to identify the most favourable binding pose, and of a subsequent molecular dynamics run which indicated a peculiar effect of the compound on the motion pattern of the transporter.

INTRODUCTION

Resistance to chemotherapy is to date the main obstacle in cancer treatment. Although the genetic and biochemical mechanisms involved in drug resistance have been widely investigated, there is an increasing awareness that the cause of therapy failure and disease relapse is in part due to tumour heterogeneity. Tumours can be defined as a "complex ecosystem" consisting of heterogeneous cells types able to create an hypoxic environment with a hierarchic organization.[1,2] Cancer stem cells (CSCs) are at the apex of this hierarchy. CSCs are a small population with great tumourigenicity, self-renewal ability and intrinsic resistance to conventional and targeted cancer therapy. Thus, CSCs intrinsic chemoresistance may be the cause of disease progression and relapse in different types of cancer.[3,4] The current antitumour strategies, either chemotherapy- or radiotherapy-based, inhibiting bulk replicating tumour cells are not efficacious *vs* CSCs owing to their multiple intrinsic mechanisms of resistance.

One of the main mechanisms of CSCs chemoresistance is the abundance of ATP Binding Cassette (ABC) transporters,[4–6] a family of transporters actively involved in the efflux of chemotherapuetic agents and targeted-therapies.

ABC transporters are structurally constituted by two nucleotide-binding domains (NBD) and two transmembrane domains (TMD).[1] The substrate binding site is placed at TMD level. It is widely accepted that ABC transporters may play a pivotal role in regulating stem cell renewal, survival, differentiation and chemoresistance.[7] The tumour-promoting activity is linked to the involvement of these transporters in the regulation of: (i) cellular redox status; (ii) release of signalling molecules and hormones; (iii) membrane lipid composition; (iv) cellular metabolism and release of nutrients and metabolites; (v) changes in tumour microenvironment.[1] Overall,

ABC proteins transport cell-signalling molecules that could maintain the tumour and promote tumourigenesis.

ABGC2/BCRP (Breast Cancer Resistance Protein) is one of the hallmark of stemness,[8] but it has a limited spectrum of substrates compared to other transporters such as ABCB1/P-glycoportein (P-gp).[9] Recently, we and others highlighted the overexpression of P-gp in SC and CSCs, where it exerts protective functions from toxic catabolites, xenobiotics and chemotherapeutic drugs.[6,10–13]. In the tumour context, blocking the activity of P-gp in CSCs will represent a promising approach to improve the chemosensitivity to different chemotherapeutic drugs in the most chemorefractory tumour component.

With this in mind, we developed a new class of P-gp ligands, starting from our previously studied P-gp inhibitor, **MC70** ([4'-(6,7-dimethoxy-3,4-dihydro-1H-isoquinolin-2-ylmethyl)biphenyl-4-ol]).[14,15] **MC70** is a potent P-gp inhibitor (EC_{50} = 0.69 μM), with moderate activity towards the Multidrug Resistance Related Protein MRP1 (EC_{50} = 9.30 μM) and breast cancer resistance protein BCRP (EC_{50} = 73 μM).

We have previously performed SAR studies on **MC70** focusing on two structural aspects: i) the functionalization of phenolic group with alkyl and oxyalkyl chains,[16] and with more complex moieties containing variously substituted furazan (1,2,5-oxadiazole) ring[17] and ii) the "decoration" of the biphenyl core.[18] The present work is a further development of the structural modulation of **MC70** and was inspired by the well-known application of bioisosteres in drug design.[19] In particular, the study was focused on the phenolic group of **MC70**: the isostere substitution was fulfilled using an NH group made "acidic" through the introduction of an electron-withdrawing moiety or through the inclusion in a heteroarene. The synthesized compounds display a variety of structural features, which determine properties of key impact on

molecular recognition: besides the possibility of preventing phenol metabolic transformations, the isosteric substitutions aimed at the improvement of activity against P-gp through wide modulation of shape, lipophilicity, steric and electronic properties. This structural tolerance has been already experienced by the authors in previous works, in which even subtle changes made on **MC70** scaffold gave rise to series of derivatives characterized by a large range of activity, and can be partially explained through the well-known polyspecifity of the target.[20]

RESULTS AND DISCUSSION

Chemistry. The synthetic routes followed in the present study are depicted in the schemes reported below. Target compounds **3a-g** (Scheme 1) and **9a-c** (Scheme 2) were synthesized according to the same path: the key step is represented by the synthesis of the diphenyl intermediates obtained through the Suzuki coupling of an appropriately built bromoarene with 4-(hydroxymethyl)benzeneboronic acid. The reaction conditions were adapted from a reported procedure:[21] the coupling reaction was conducted in aqueous media in presence of an excess of diisopropylamine and using a ligand-free catalyst (palladium (II) acetate). The products of the coupling reaction were then converted to the corresponding benzylic chlorides which were readily reacted with 6,7-dimethoxy-1,2,3,4-tetrahydroisoquinoline in mild conditions.

In the case of compounds **5a** and **6** the coupling reaction between the functionalized bromoarene and the boronic acid, carried out in several conditions, afforded only traces of the desired compounds; the two products were thus obtained through the functionalization of the aniline group after the introduction of dimethoxytetrahydroisoquinoline moiety (Scheme 1). As for the synthesis of **6**, the reaction of aniline intermediate with phenylsulfonyl chloride gave the (N-phenylsulfonyl)phenylsulfonamido- derivative **5b**, which was subsequently converted to **6** through basic hydrolysis. (Scheme 1).

Scheme 1. Synthesis of compounds 3a - g, 5a, 5b and 6[a]

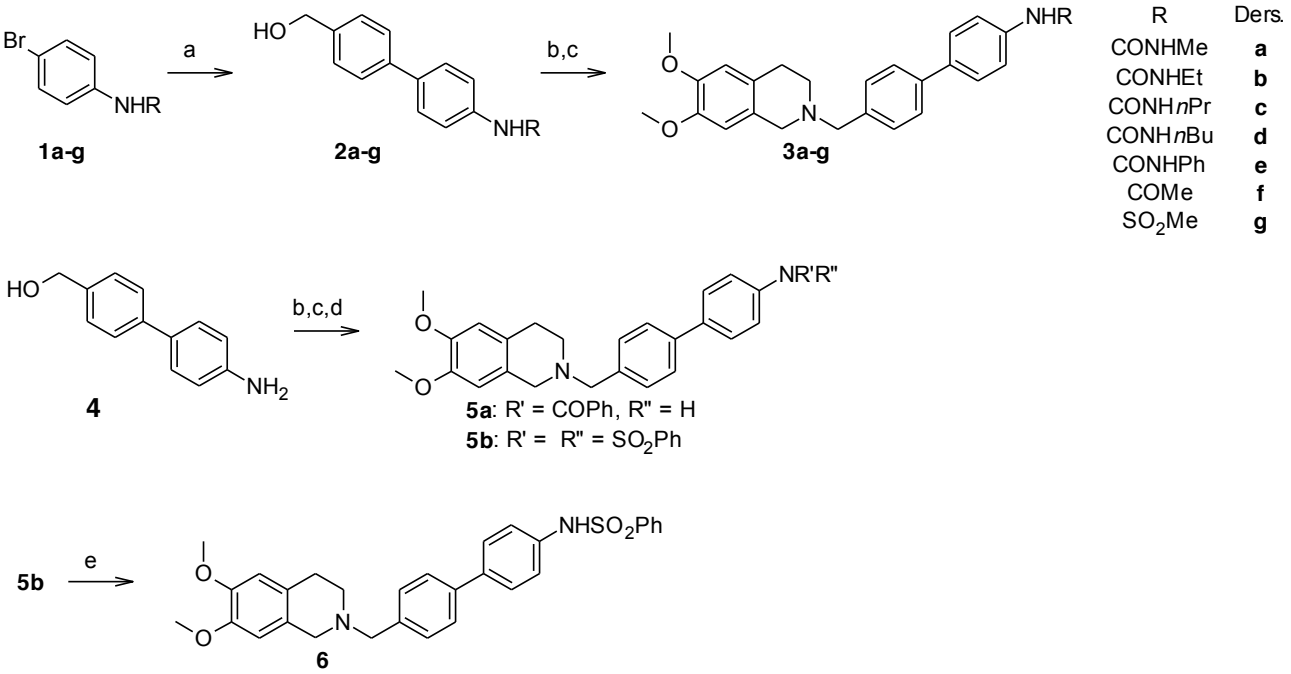

[a]Reagnets and Conditions: (a) 4-(hydroxymethyl)benzeneboronic acid, *i*Pr_2NH, $Pd(OAc)_2$, H_2O, 80 °C; (b) 37% HCl, 90 °C; (c) 6,7-dimethoxy-1,2,3,4-tetrahydroisoquinoline hydrochloride, Et_3N, CH_3CN, 60 °C; (d) Et_3N, PhCOCl (for **5a**) or $PhSO_2Cl$ (for **5b**), CH_2Cl_2, room temperature; (e) LiOH, DMF, 120 °C.

Scheme 2. Synthesis of compounds 9a - c, 11, 12, 15, 17, 18 and 20a

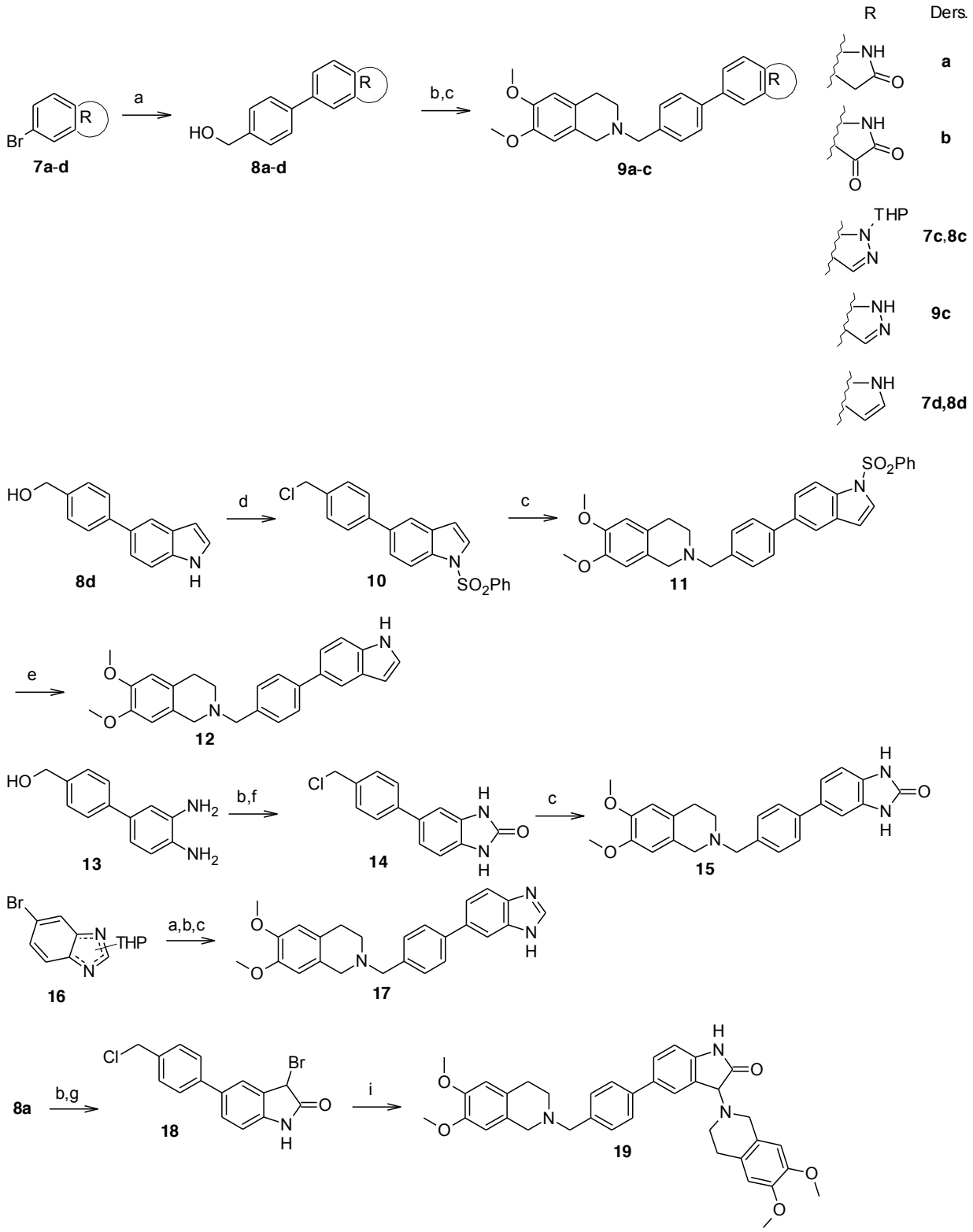

[a]Reagents and Conditions: (a) 4-(hydroxymethyl)benzeneboronic acid, *i*Pr_2NH, $Pd(OAc)_2$, H_2O, 80 °C; (b) 37% HCl, 90 °C; (c) 6,7-dimethoxy-1,2,3,4-tetrahydroisoquinoline hydrochloride, Et_3N, CH_3CN, 60 °C; (d) $PhSO_2Cl$, NaOH, catalytic *n*Bu_4NHSO_4, 1,2-dichloroethane, 70 °C; (e) NaOH, tetrahydrofuran/CH_3OH 2/1, reflux; (f) triphosgene, Et_3N, CH_2Cl_2, room temperature; (g) bromotrimethylsilane, DMSO, tetrahydrofuran, 0 °C to room temperature; (i) 6,7-dimethoxy-1,2,3,4-tetrahydroisoquinoline hydrochloride, $KHCO_3$, CH_3CN, 0 - 10 °C.

In case of indole derivative **12**, the Suzuki coupling product was reacted with phenysulfonyl chloride, affording the N-phenylsulfonyl benzylic chloride **10** as result of the nucleophilic substitution of the benzylic sulfonate by chloride ions formed *in situ* (Scheme 2).

Compound **15** was synthesized starting from intermediate **13**:[22] also in this case coupling reaction carried out on the bromoarene with imidazolone moiety could not afford the desired product in useful yields; for this reason, intermediate **13** was converted to the benzylic chloride and readily reacted with triphosgene in mild conditions (Scheme 2).

Benzimidazole compound **17** was obtained starting from the mixture of isomers **16**:[23] the isomers coming from coupling reaction were not separated and were reacted with concentrated hydrochloric acid, giving concomitant deprotection of the tetrahydropiranyl group and conversion to benzylic chloride, which was then substituted with 6,7-dimethoxy-1,2,3,4-tetrahydroisoquinoline (Scheme 2).

Compound **19** was obtained through a double nucleophilic substitution with 6,7-dimethoxy-1,2,3,4-tetrahydroisoquinoline in very mild conditions on intermediate **18**. The latter was synthesized using an oxidative bromination procedure, reported in Kajita et al.,[24] in presence of borotrimethylsilane and dimethylsulfoxide (Scheme 2).

Biology

P-gp interacting profile and ABC transporters selectivity

All the compounds were tested for their P-gp interacting profile by three combined assays: *i)* inhibition of the transport of a pro-fluorescent probe (Calcein-AM) in MDCK-MDR1 cells; ii) Apparent Permeability (P_{app}) determination (BA/AB) in Caco-2 cell monolayer; *iii*) ATP cell depletion in MDCK-MDR1 cells. As previously reported, the first assay measures the potency of the interaction of each ligand towards P-gp. The second assay measures the ratio between two fluxes: 1) BA, representative of passive diffusion, from the basolateral to apical compartments, and (2) AB, representative of active transport, from the apical to basolateral compartment.

If BA/AB is < 2, the compound can be considered as an inhibitor, if BA/AB > 2, the compound is classified as a substrate. This last information is completed by the third assay (ATP cell depletion), that measures the total ATP cell level in the MDCK cells overexpressing only MDR1: in this setting the observed effect can be mainly ascribed to the overexpressed transporter.

Only a P-gp unambiguous substrate (category I), as transported by the pump, induces an ATP consumption, while a P-gp inhibitor does not induce ATP consumption. Compounds displaying a BA/AB > 2 but not inducing an ATP cell depletion are classified as class IIB3 substrates.[25]

Moreover, to assess the selectivity of all compounds, their activity towards the other two MDR sister proteins, MRP1 and BCRP, has been detected by measuring the inhibition of the efflux of Calcein-AM (MRP1 substrate) in cells overexpressing MRP1 (MDCK-MRP1 cells) and of the fluorescent probe Hoechst 33342 (BCRP substrate) in cells overexpressing BCRP (MDCK-BCRP cells).

As shown in Table 1, all compounds were active towards P-gp with EC_{50} values ranging from 0.015 to 29.5 μM, except for derivative **5a** that was completely inactive towards all the MDR proteins.

With respect to the reference compound **MC70** (EC_{50} = 0.69 μM), all the developed compounds were found less active (**3a-c**, **3f**, **3g**, **9a**, **9b**, **11**, **12**, **15**, **17**, **19**) or displaying comparable activity (**9c**, **6**, **3e**). Only compound **5b**, bearing a *N*-(benzenesulfonyl)benzenesulfonamide moiety, was potent and selective towards P-gp (EC_{50} = 15 nM).

All compounds were selective towards P-gp and showed a category IIB3 substrate profile since the Apparent Permeability P_{app} (BA/AB) values were > 2 for all compounds and they were all unable to induce ATP cell depletion.

The only exception was compound **12**, which displayed a weak P-gp inhibitor profile having a P_{app} < 2, not inducing an ATP consumption and exerting a low P-gp inhibiting effect (EC_{50} = 21.2 μM).

Table 1. Biological Activity Profile of Target Compounds.

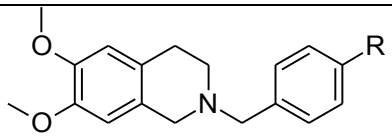

Compound	R	EC_{50} ± SEM (μM)[a]			ATP	P_{app}[b]
		MDR1	MRP1	BCRP		
3a	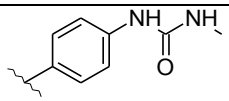	3.1 ± 0.60	NA	NA	NO	12.8
3b	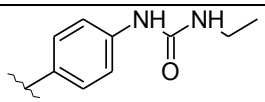	1.7 ± 0.32	NA	NA	NO	9.3
3c	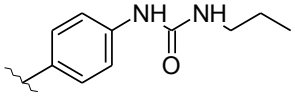	1.1 ± 0.20	NA	NA	NO	17.6
3d	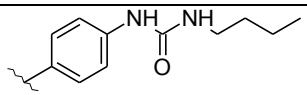	0.32 ± 0.06	NA	46 ± 9.20	NO	12.8

3e	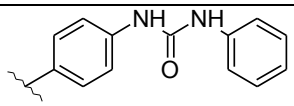	0.98 ± 0.20	NA	NA	NO	> 20
3f	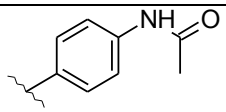	1.52 ± 0.30	NA	NA	NO	13.6
3g	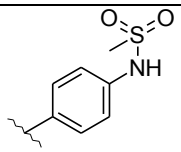	5.2 ± 1.00	NA	NA	YES	5
5a	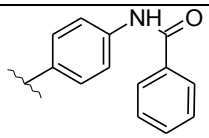	NA	NA	NA	NO	19.9
5b	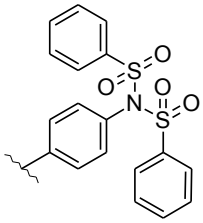	0.0153 ± 0.003	NA	NA	NO	> 20
6	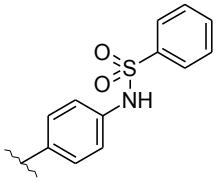	0.87 ± 0.20	NA	NA	NO	15
9a	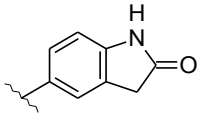	1.47 ± 0.30	NA	NA	NO	3.6
9b	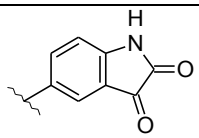	21.4 ± 4.20	NA	NA	NO	8.1
9c	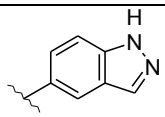	0.90 ± 0.10	NA	NA	NO	12
11	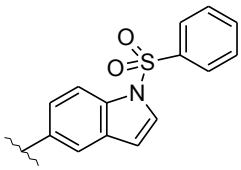	19.2 ± 3.80	NA	NA	NO	4.2

12	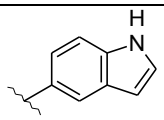	21.2 ± 4.20	NA	NA	NO	1.9
15	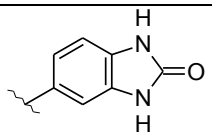	29.5 ± 5.78	NA	NA	NO	15
17	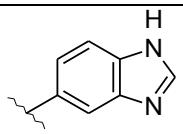	6.93 ± 1.30	NA	NA	NO	9.2
19	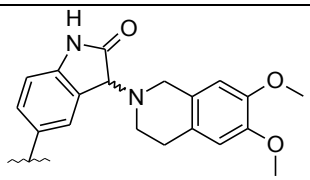	1.2 ± 0.24	NA	1.8 ± 0.30	NO	8.5
MC70[15]	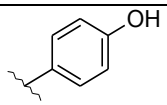	0.69	9.30	73	NO	1.3

[a] Values are the means ± SEM of three independent experiments carried out in triplicate.

[b] Apparent permeability ratio (the value is from two independent experiments).

Co-administration assay

Compound **5b**, displaying the best P-gp activity profile (EC_{50} = 15nM), has been tested in a co-administration assay in order to study its ability to revert MDR, restoring Doxorubicin cytotoxic effect in MDCK-MDR1 cells.

Doxorubicin alone did not exert cytotoxicity being a P-gp substrate, while in presence of 1 μM of compound **5b**, it was able to induce cell death. Compound **5b** was tested at different doses in a range near its EC_{50} value and showed the best reverting activity at 1 μM as depicted in Figure 1. To exclude any effect of 1% v/v of DMSO, the solvent used to dissolve **5b**, we preliminarily tested that cells treated with Doxorubicin with or without 1% v/V of DMSO did not differ in their drug content (data not shown) .

Figure 1. In vitro cell growth experiments performed on MDCK-MDR1 cells in presence of 10 μM Doxorubicin, Doxo, alone (white bar), compound **5b** at different doses, alone and in co-administration of Doxo. ~~DMSO 1% v/v was the concentration of solvent present in cells treated with compound **5b**.~~ Each bar represents the mean ± SEM of two experiments performed in triplicate. One-way ANOVA analysis: ***$p < 0.0005$, ****$p < 0.0001$ *vs* control.

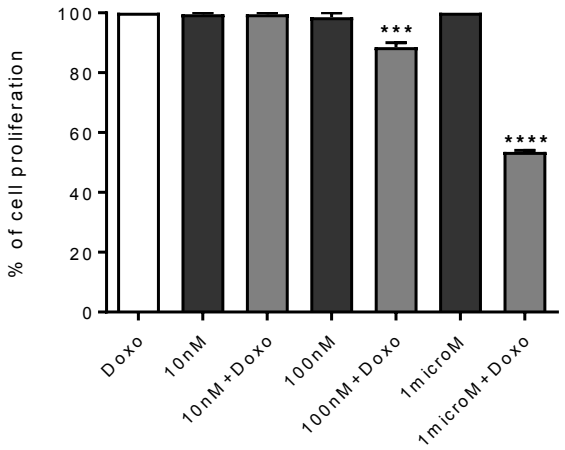

Efficacy of compound 5b against P-gp-expressing cancer stem cells

Given the central role of CSCs in mediating drug resistance in tumours, and the emerging role of ABC transporters in the drug resistance of CSCs, we tested the efficacy of compound **5b** against primary CSCs, in order to assay its activity in a model closer to the biology of patients' tumours. We focused on glioblastoma (GB) and malignant pleural mesothelioma (MPM), two tumours that differ for pathogenesis, genetic background and histological origin, but share a high chemoresistance due to CSCs component.[3,26] From three patients affected by GB and MPM we separated the differentiated cells (GDC or MDC, respectively) from the SCs of the same tumour (GSC or MSC, respectively), as detailed in the Supporting Information. The phenotypic characterization of DC and SC are reported in the Supplementary Tables S1 and S2. By

screening the expression levels of ABC transporters in SC versus DC, several ABC transporters involved in drug resistance were found significantly more expressed in SC compared to DC. ABCB1/P-gp/Mdr1, ABCB2/Mdr2, ABCC1/MRP1 and ABCG2/BCRP were significantly more expressed in 3 out of 3 SC patients in both GB and MPM (Figure 2A). Given the high specificity of compound **5b** for inhibiting P-gp, we focused on this transporter. The high expression of P-gp at protein levels in GSC and MSC compared to GDC and MDC was validated by immunoblotting (Figure 2B).

Figure 2. Expression of ABC transporters in human cancer stem cells of glioblastoma and mesothelioma. Differentiated cells from primary glioblastoma (GDC1-3) and mesothelioma (MDC1-3) from 3 patients and stem cells from the same patients (GSC1-3 and MSC1-3) were isolated and put in culture. **A.** Hitmap of ABC transporters, represented in a colorimetric logarithmic scale. The expression of the each gene in the corresponding DC was considered 1 (not shown in the figure). **B.** Immunoblotting analysis of P-gp expression in DC and SC of each patient. Actin was used as control of equal protein loading.

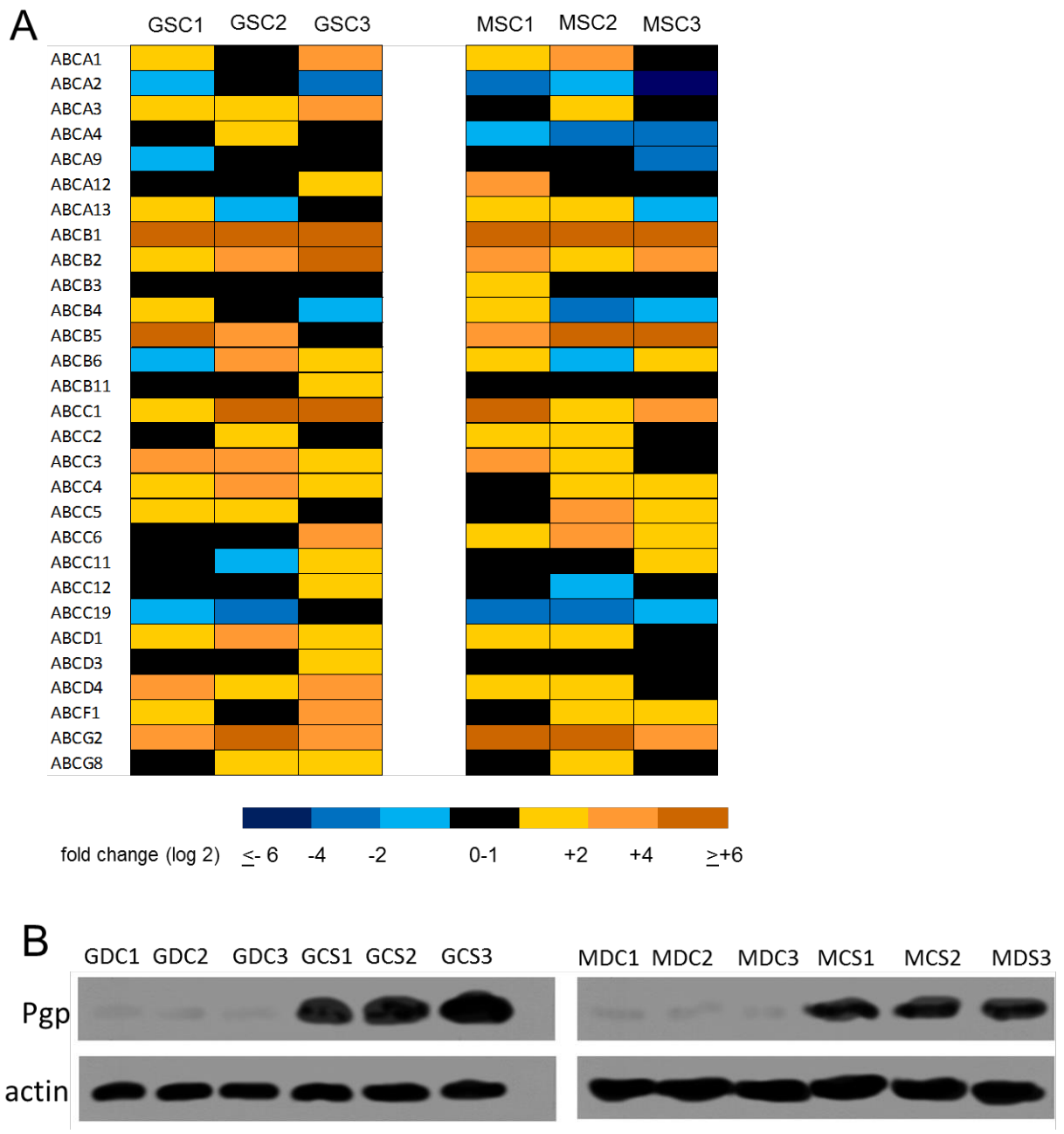

In line with this pattern, GDC and MDC accumulated more Doxorubicin, a substrate of P-gp, than GSC and MSC (Figure 3A-D). The third-line generation P-gp inhibitor Elacridar significantly increased Doxorubicin accumulation at low micromolar concentration, in line with its K_i[14] (Figure 3B and Figure 3C) in SC. This effect was stronger in SC than in DC of both

tumours (Figure 3A-D), consistently with the higher expression of P-gp in SC. Notably, compound **5b** produced an analogue increase of Doxorubicin at nanomolar concentration (Figure 3A-D) in SC of both tumours.

Figure 3. Intracellular Doxorubicin accumulation in human cancer stem cells of glioblastoma and mesothelioma. Differentiated cells from primary glioblastoma (GDC, panel **A**) and mesothelioma (MDC, panel **C**) from 3 patients and stem cells from the same patients (GSC, panel **B**, and MSC, panel **D**) were incubated for 3 h with medium containing 5 μM Doxorubicin (Doxo), alone or with the indicated concentrations of Elacridar or compound **5b**. DMSO 1% v/v was the concentration of solvent present in cells treated with compound **5b**. The intracellular accumulation of Doxorubicin was measured spectrofluorimetrically in duplicates (n=3). Data are means ± SEM of each cell categories. One-way ANOVA analysis: $*p < 0.05$ Elacridar or compound **5b** + Doxo *vs* Doxo; $**p < 0.005$ Elacridar or compound **5b** + Doxo *vs* Doxo; $***p < 0.0001$ compound **5b**+Doxo *vs* Doxo.

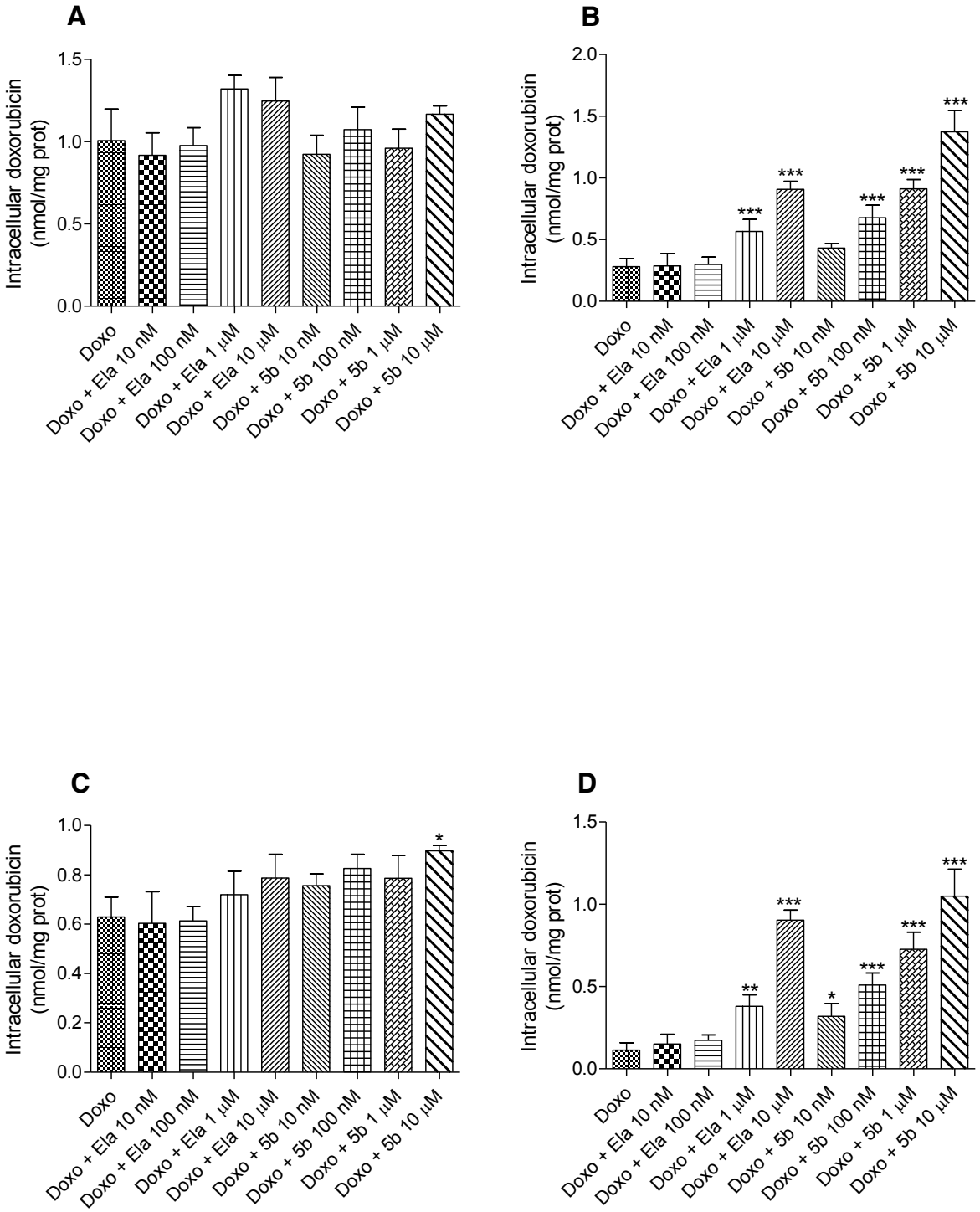

In line, with this trend, compound **5b** enhanced the acute cytotoxicity, measured as release of lactate dehydrogenase (LDH) (Supporting Figure 1A-B), and reduced cell viability (Figure 4A-

B) induced by Doxorubicin in SC, where Doxorubicin alone was ineffective, as a consequence of its low intracellular accumulation. Again, the effect of compound **5b** on these parameters was achieved at 10 nM, while Elacridar produced the same effects at 1 μM. Overall, these results pointed out that compound **5b** was more effective than the most potent P-gp inhibitor presently used in preclinical models and in clinical trials. According to the in vitro results, the compound was not toxic when used alone. To exclude any effect of DMSO 1% v/v, the solvent used to dissolve **5b**, we checked that at this concentration DMSO did not change the doxorubicin accumulation (Figure 3A-D), nor the cell damage (Supporting Figure S1A-B) or the cell viability (Figure 4A-B) also in primary cells.

Figure 4. Viability of cancer stem cells of glioblastoma and mesothelioma in the presence of compound 5b and Doxorubicin. Differentiated cells from primary glioblastoma (GDC) and stem cells from the same patients (GSC, panel **A**), differentiated cells from primary mesothelioma (MDC) and stem cells from the same patients (MSC, panel **B**) were incubated for 72 h with fresh medium (ctrl) or medium containing 5 μM Doxorubicin (doxo), alone or 10 nM compound **5b** or 1 μM Elacridar. DMSO 1% v/v was the concentration of solvent present in cells treated with compound **5b**. Cell viability was measured by a chemiluminescence-based assay in quadruplicates (n=3). Data are means ± SEM of each cell categories. One-way ANOVA analysis: ***$p < 0.0001$ Doxo or Elacridar or compound **5b** *vs* ctrl; °° < 0.0002 Elacridar or compound **5b** *vs* Doxo alone; °°°$p < 0.0001$ Elacridar or compound **5b** *vs* Doxo alone.

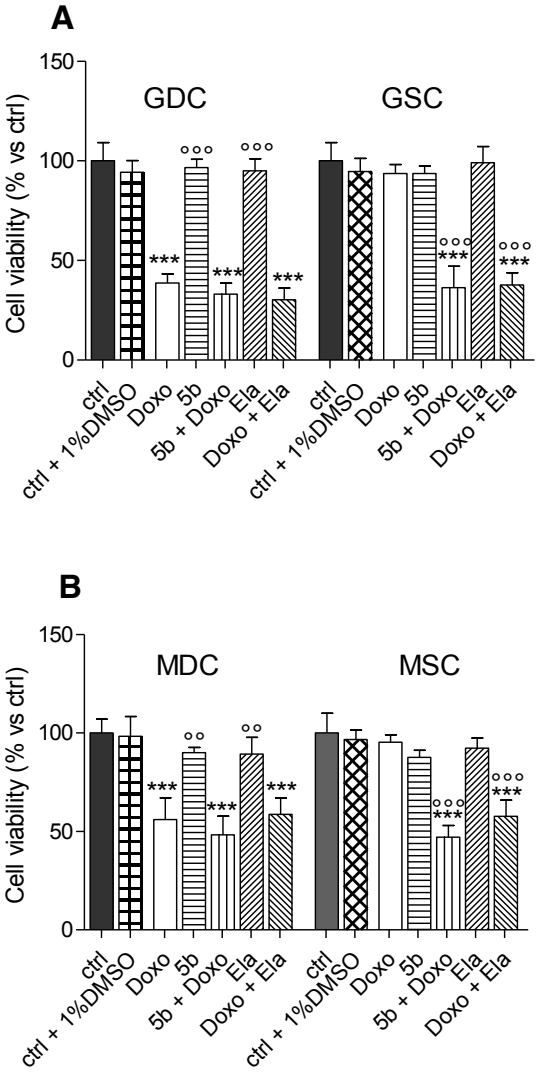

Although the absence of toxicity must be proved in *in vivo* experiments, that are ongoing in our laboratory, this data suggests that compound **5b** achieves good efficacy at low concentrations and thus can be less affected by the side-effects characterizing all the P-gp inhibitors tested until now, including Elacridar.[27]

Compound **5b** did not increase the toxicity of Doxorubicin in DC, in keeping with the absence or very low level of P-gp in these cells. This data indirectly confirms that the compound is a specific modulator of P-gp.

To further prove this point, since SC express different ABC transporters, we stably knocked-down P-gp in GSC and MSC derived from one patient, using a CRISR-Cas vector. Knocked-out (KO) SCs had undetectable P-gp, in line with DC of the corresponding patient (Figure 5A).

Figure 5. Effects of compound 5b on cancer stem cells of glioblastoma and mesothelioma knocked-out for P-gp. Stem cells from glioblastoma patients #2 (GSC) and from mesothelioma patient #1 (MSC) were not untreated (nt) or transfected with a scrambled CRISPR-Cas vector (scr) or with a CRISPR-Cas vector knocking-out P-gp (KO). Glioblastoma and mesothelioma differentiated cells (GD and MD) of the same patient were included as control of P-gp-lowly expressing cells. **A.** Immunoblotting analysis of P-gp expression in DC and SC of each patient. Actin was used as control of equal protein loading. **B-C.** Cells were incubated for 3 h with medium containing 5 μM Doxorubicin (Doxo), alone or with 10 nM compound **5b**. The intracellular accumulation of Doxorubicin was measured spectrofluorimetrically in duplicates (n=3). Data are means ± SEM of each cell categories. One-way ANOVA analysis: *$p< 0.05$ compound **5b** + Doxo *vs* Doxo GSC/MSC nt; **$p< 0.005$ compound **5b** + Doxo *vs* Doxo GSC/MSC nt;°°° $p< 0.0008$ compound **5b**-treated KO cells *vs* compound **5b**-treated nt or scr-cells, °° $p< 0.007$ compound **5b**-treated KO cells *vs* compound **5b**-treated nt or scr-cells.

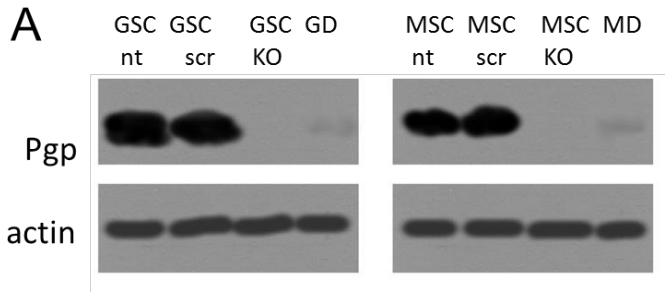

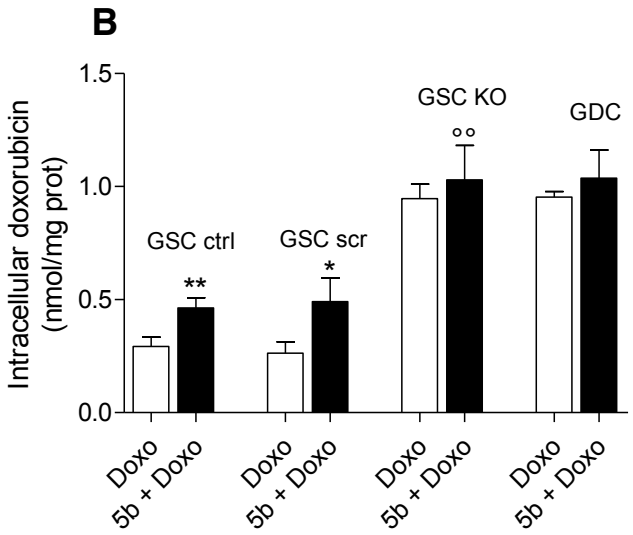

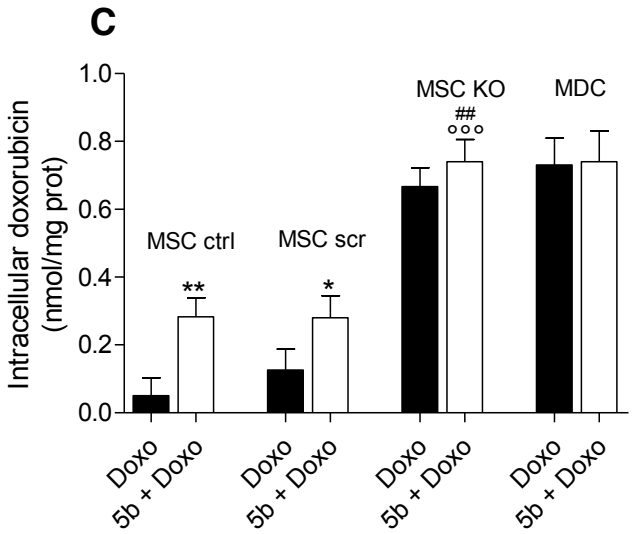

Compared to untreated SC or SC treated with a not-targeting (scrambled) CRISR-Cas vector, used as internal control of specificity, KO SC of both GB and MPM accumulated significantly more doxorubicin (Figure 5B-C) and the amount of doxorubicin was similar to GD or MD, respectively. Compound **5b**, that increased the cytotoxic effects of doxorubicin in terms of reduced viability in untreated and scrambled-treated SC (Supplementary Figure S2A-B), was devoid of effects in KO cells. This further supports the previous evidences that compound **5b** effects were specifically mediated by the interaction with P-gp.

Molecular modelling

In the attempt to give a reasonable hypothesis of binding mode and thus to possibly rationalize activity data towards P-gp for the most active compound of the series (**5b**), a molecular dynamics study was fulfilled. For comparison, a similar study was carried out for the structurally correlated compound **6**, which displayed an EC_{50} almost sixty-fold higher than **5b**. The study consisted in a well-tempered metadynamics simulation,[28] which allowed to gain a sound hypothesis of binding mode for the two compounds exploring the free energy surface of the systems through the application of a bias potential on selected collective variables. In the present work the collective variables were designed in order to describe the position and the orientation of the ligands inside the internal cavity formed by the transmembrane (TMs) helices, which is the region comprising the ligand binding site. To this aim the collective variables were selected as follows: i) the distance *d* between the centre of mass of the ligand and the centre of mass of Leu971; ii) the torsion angle χ formed by the benzylic carbon of the biphenyl moiety of the ligands, the nitrogen atom of the N-sulfonyl moiety of the ligands, the centre of mass of Leu971 and the centre of mass of Gln986: the latter two points approximately overlap the principal axis of the macromolecule (Figure S3).

The free energy surface (FES) resulting from simulation of the system including **5b** is reported in Figure 6.

Figure 6. Free energy surfaces reconstructed from well-tempered metadynamics for complex involving compound 5b. Free energy values are reported in $kJ \cdot mol^{-1}$.

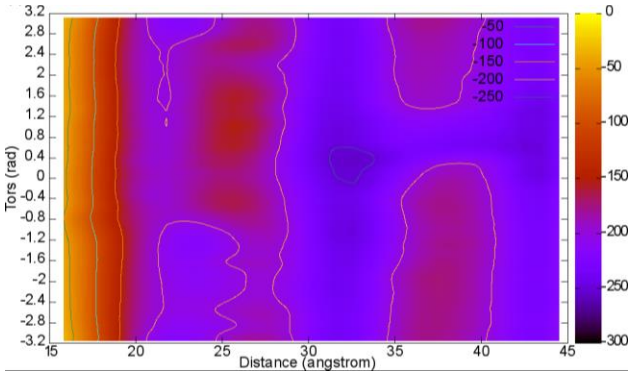

Even though the free energy surface is rather shallow, a minimum is identified corresponding to the basin at $d \approx 32$ Å and $\chi \approx 0.3$ rad. A representative structure for this basin, obtained through cluster analysis of selected frames, is reported in Figure 7A and B.

Figure 7. A. Representation of the complex corresponding to the minimum energy basin for compound 5b. B. Relevant interactions of 5b in the binding site. (PDB ID: 4Q9H).

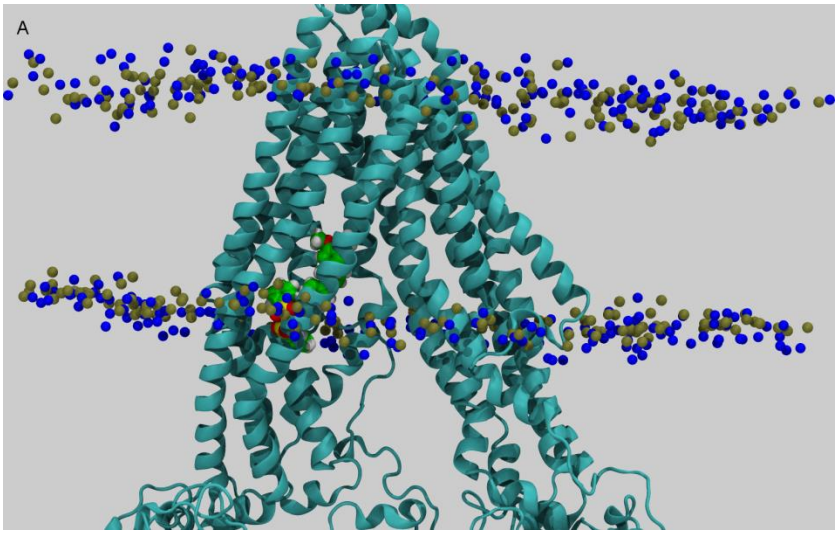

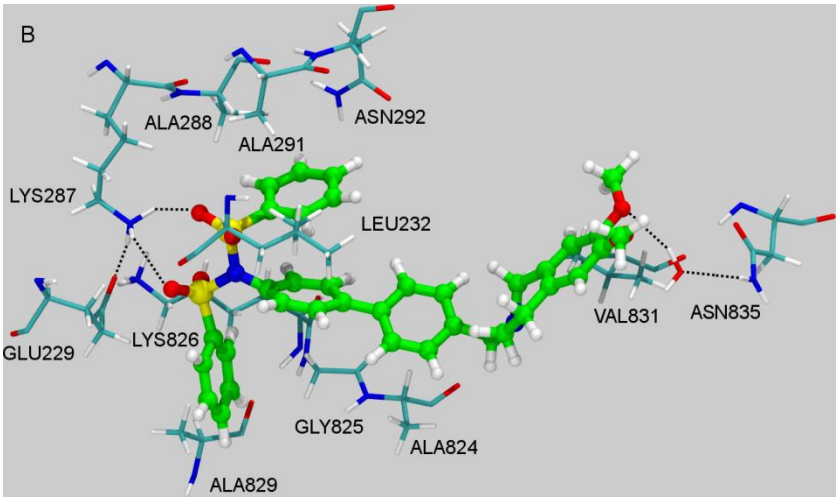

As can be seen from the representation in Figure 7B, the putative binding site is a strongly hydrophobic pocket in which the interactions involve mainly side chains and backbone atoms of the protein residues belonging to TM4, TM5, TM9 and TM10. Besides these, the complex is characterized by the presence of several hydrogen bonds as depicted in Figure 7B.

In the case of compound **6**, from the free energy surface (Figure S4) several basins can be identified: of these basins, A and B were taken in consideration for comparison with compound **5b**, in view of their free energy values and of the corresponding positions of the ligand, still lying inside the internal cavity. The protein domains involved in the formation of the two complexes belong to TM4, TM5, TM6 and TM9 and also in these cases the complexes show a mainly hydrophobic pattern with additional polar interactions (Figure S5A, B and Figure S6A, B).

The three structures were subsequently subdued to an unbiased 50 ns molecular dynamics run in order to investigate stability and dynamic properties of the complexes. The inspection of the trajectories indicated that ligand **5b** proved quite stable and ligand **6** in the complex B reached stability after 5 ns (see ligand root mean square deviation plot in supplementary Figure S7). Complex A of compound **6** was characterized by a weaker stability, with a significant increase of RMSD after 20 ns: Figure 8 shows the comparison of the initial pose of basin A (green), the final

pose of the 50 ns trajectory (pink) and the pose representative of the large basin C (blue); as can be seen, at the end of the trajectory, compound **6** has moved towards the cytoplasmic side, partially egressing from the inner cavity of the protein and approaching a pose similar to that corresponding to basin C. Even though it is established that dynamic properties are not directly inferable from metadynamics simulations,[29] taken together the shape of the free energy surface in the region considered and the dynamic behaviour of compound **6** during the unbiased run suggest that basin A could possibly represent the starting configuration for the egression path from the interval cavity.

Figure 8. Poses for compound 6 extracted from metadynamics simulation (green liquorice representation) and at the end of the unbiased 50 ns trajectory (pink liquorice representation). For comparison also the pose corresponding to free energy basin C is reported (blue liquorice representation). (PDB ID: 4Q9H).

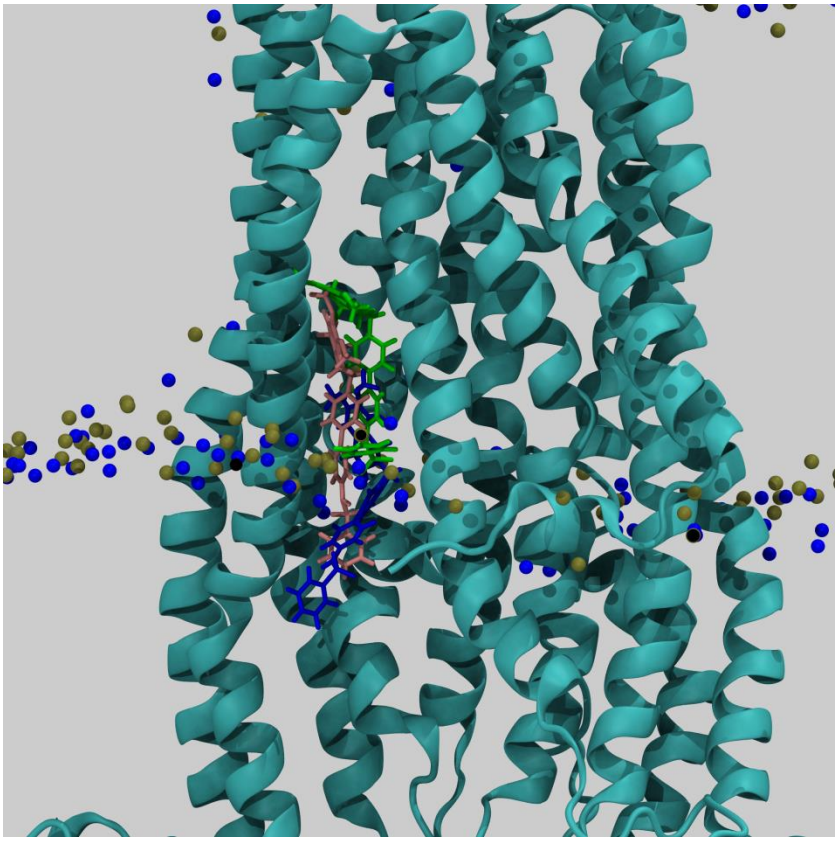

On the basis of the above considerations, further comparison was fulfilled on trajectories involving complex with **5b** and **6**-B: in order to hypothesize the possible conformational effects of the binding of the ligands, a principal component analysis was fulfilled over the two trajectories using ProDy.[30] Figure 9 reports the comparison of root mean square fluctuations (RMSF) of the C_α of the protein, corresponding to the first component of the motion for the two trajectories; a pictorial representation of the vector for the two trajectories is reported in Figure 10 (A for compound **5b** and B for compound **6**).

From the analysis of the RMSFs a clear difference emerges, in that complex **5b** displays a definitely larger mobility in the regions of the two nucleotide binding sites (NBDs).

Figure 9. Comparison of root mean square fluctuations of the C_α of protein obtained for the first mode of motion of complex with compound 5b and 6-B in the unbiased simulation.

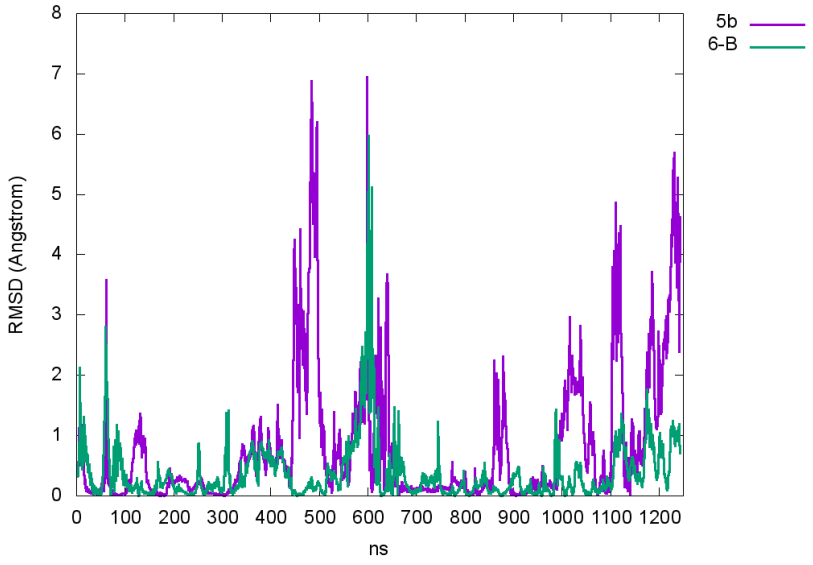

Moreover, the representations of the vector reported in Figure 10, indicate that for the complex with compound **6** the motion of the NBDs is mainly a rotation around the principal axis of the protein, whilst, in the case of complex with **5b**, the displacement occurs in the plane of the protein and leads to a larger distance fluctuation between the NBDs: this motion is considered pivotal in priming the efflux of ligands form the internal cavity of P-gp.[31,32]

Figure 10. Representation of the vector describing the first mode of motion extracted from the unbiased simulation for compound 5b (A) and for compound 6-B (B).

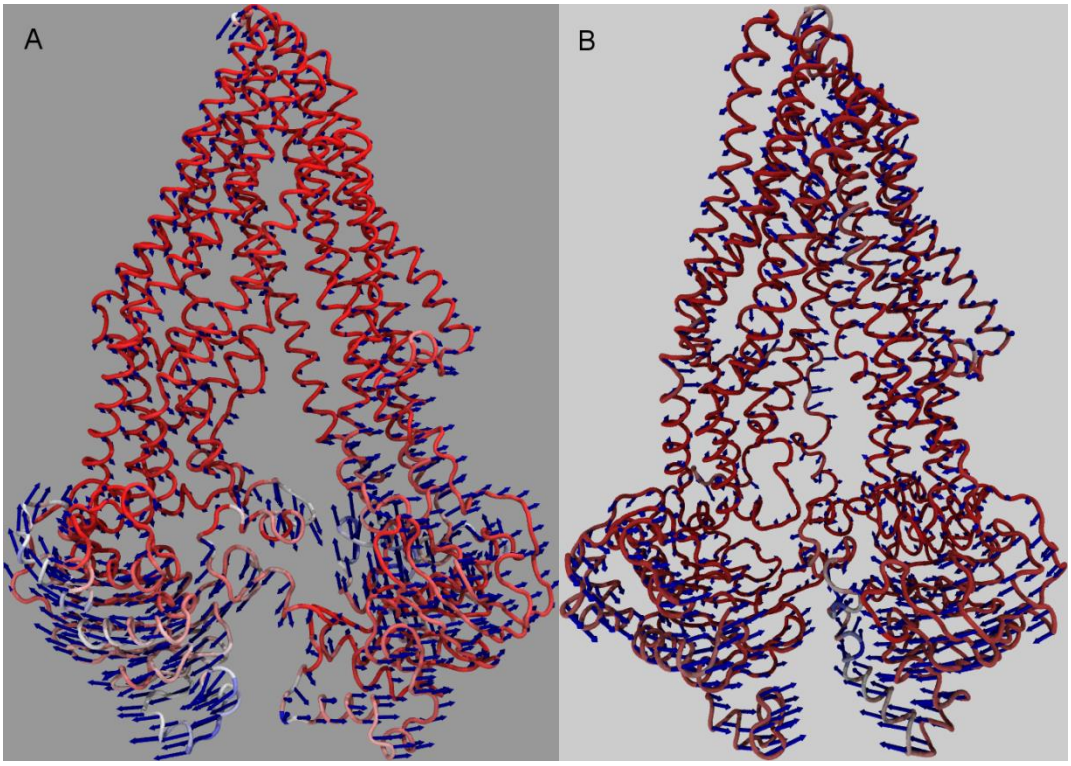

Taken together, the results of the molecular modelling study produce a consistent hypothesis of interaction between the two ligands and P-gp, and allow a reasonable explanation for the difference in the EC_{50} values.

CONCLUSIONS

Overall, we identified compound **5b** as a specific P-gp ligand, with a potency comparable to Elacridar, devoid of any toxicity when used alone but able to increase significantly the toxicity of P-gp substrates such as Doxorubicin. Noteworthy, compound **5b** was of particular interest because it reversed the chemoresistance mediated by P-gp in CSCs, the hardest tumour component to be eradicated. The effect was not tumour specific, since it was achieved on two models – the glioblastoma multiform and the malignant pleural mesothelioma – with completely different pathogenesis, mutational profile and histological origin, but with a high chemoresistance to most chemotherapeutic drugs.

Compound **5b** was also the object of a molecular modelling study, in comparison with the structurally related **6**, which allowed a deeper understanding of the molecular basis of the activities of the two compounds: through a well-tempered metadynamics simulation the most favourable binding mode for the two compounds was envisaged, revealing a pattern of hydrophobic interactions which, particularly in the case of **5b**, were enriched by additional hydrogen bonds. Moreover, the analysis of the unbiased trajectories revealed different motion patterns of the protein for the two compounds, indicating a more pronounced efflux-characteristic motion for compound **5b**.

Targeting the CSCs in tumours, in particular overcoming their multidrug resistant phenotype, is a still unmet need, but it may represent a sure advantage in cancer treatment. The identification of compound **5b** is a step forward in this direction.

EXPERIMENTAL SECTION

Chemistry

The purity of target compounds was assessed by RP-HPLC. Analyses were performed on a HP1100 chromatograph system (Agilent Technologies, Palo Alto, CA, USA) equipped with a quaternary pump (G1311A), a membrane degasser (G1379A), a diode-array detector (DAD) (G1315B) integrated in the HP1100 system. Data analysis were processed by HP ChemStation system (Agilent Technologies). The analytical column was a LiChrospher® 100 C18-e (250×4.6mm, 5µm) (Merck KGaA, 64271 Darmstadt, Germany) eluted with CH_3CN/H_2O 0.1% TFA in a ratio depending on the characteristics of the compound. All compounds were dissolved in the mobile phase at a concentration of about 0.1 mg/ml and injected through a 20 µL loop. UV signals were recorded at 210, 226 and 254 nm (with 360 nm as reference wavelength) and the purity of the test samples was evaluated as a percentage ratio between the areas of the main peak

and of possible impurities at the three wavelengths and also using DAD purity analysis of the chromatographic peak. For all target compounds purity resulted > 95% (see Supporting information for details).

Biology

Materials. Cell culture reagents were purchased from Celbio s.r.l. (Milano, Italy). CulturePlate 96/wells plates were purchased from PerkinElmer Life Science (Waltham, MA) and Falcon (BD Biosciences, Bedford, MA). Calcein-AM, bisBenzimide H 33342 trihydrochloride were obtained from Sigma-Aldrich (Milan, Italy). Electrophoresis reagents were from Bio-Rad Laboratories (Hercules, CA). The protein content of cell monolayers and cell lysates was assessed with the bicinchoninic acid kit (Sigma Aldrich). The other reagents were purchased from Sigma Aldrich.

Cell cultures. MDCK-MDR1, MDCK-MRP1 and MDCK-BCRP cells are a gift of Prof. P. Borst, NKI-AVL Institute, Amsterdam, The Netherlands. MDCK cells were grown in DMEM high glucose supplemented with 10% fetal bovine serum, 2 mM glutamine, 100 U/mL penicillin, 100 μg/mL streptomycin, in a humidified incubator at 37 °C with a 5 % CO_2 atmosphere. Caco-2 cells were a gift of Dr. Aldo Cavallini and Dr. Caterina Messa from the Laboratory of Biochemistry, National Institute for Digestive Diseases, "S. de Bellis", Bari (Italy).

Calcein-AM experiments. These experiments were carried out as described by Capparelli et al.[25] with minor modifications. Each cell line (30,000 cells per well) was seeded into black CulturePlate 96/wells plate with 100 μL medium and allowed to become confluent overnight. 100 μL of test compounds were solubilized in culture medium and added to monolayers, with final concentrations ranging from 0.1 to 100 μM. 96/Wells plate was incubated at 37 °C for 30 min. Calcein-AM was added in 100 μL of Phosphate Buffered Saline (PBS) to yield a final

concentration of 2.5 μM and plate was incubated for 30 min. Each well was washed 3 times with ice cold PBS. Saline buffer was added to each well and the plate was read with Victor3 (PerkinElmer) at excitation and emission wavelengths of 485 nm and 535 nm, respectively. In these experimental conditions Calcein cell accumulation in the absence and in the presence of tested compounds was evaluated and fluorescence basal level was estimated with untreated cells. In treated wells the increase of fluorescence with respect to basal level was measured. EC_{50} values were determined by fitting the fluorescence increase percentage versus log[dose].

Hoechst 33342 experiment. These experiments were carried out as described by Capparelli et al.[25] with modifications. Each cell line (30,000 cells per well) was seeded into black CulturePlate 96/wells plate with 100 μL medium and allowed to become confluent overnight. 100 μL of test compounds were solubilized in culture medium and added to monolayers, with final concentrations ranging from 0.1 to 100 μM. 96/Wells plate was incubated at 37 °C for 30 min. Hoechst 33342 was added in 100 μl of Phosphate Buffered Saline (PBS) to yield a final concentration of 8 μM and plate was incubated for 30 min. The supernatants were drained and the cells were fixed for 20 min under light protection using 100 μL per well of a 4% PFA solution. Each well was washed 3 times with ice cold PBS. Saline buffer was added to each well and the plate was read with Victor3 (PerkinElmer) at excitation and emission wavelengths of 340/35 nm and 485/20 nm, respectively. In these experimental conditions, Hoechst 33342 accumulation in the absence and in the presence of tested compounds was evaluated and fluorescence basal level was estimated with untreated cells. In treated wells the increase of fluorescence with respect to basal level was measured. EC_{50} values were determined by fitting the fluorescence increase percentage versus log[dose].

ATPlite assay. The MDCK-MDR1 cells were seeded into 96-well microplate in 100 μL of complete medium at a density 2 × 104 cells/well.[25] The plate was incubated overnight (O/N) in a humidified atmosphere 5% CO_2 at 37 °C. The medium was removed and 100 μL of complete medium either alone or containing different concentrations of test compounds was added. The plate was incubated for 2h in a humidified 5% CO_2 atmosphere at 37 °C. 50 μL of mammalian cell lysis solution was added to all wells and the plate shaked for five minutes in an orbital shaker. 50 μL of substrate solution was added to all wells and the plate shaked for five mitutes in an orbital shaker. The plate was dark adapted for ten minutes and the luminescence was measured.

Permeability Experiments. Preparation of Caco-2 monolayer. Caco-2 cells were seeded onto a Millicell® assay system (Millipore), where a cell monolayer is set in between a filter cell and a receiver plate, at a density of 10,000 cells/well.[14] The culture medium was replaced every 48 h and the cells kept for 21 days in culture. The Trans Epithelial Electrical Resistance (TEER) of the monolayers was measured daily, before and after the experiment, using an epithelial voltohmmeter (Millicell® -ERS). Generally, TEER values greater than 1000 Ω for a 21 day culture, are considered optimal.

Drug transport experiment. After 21 days of Caco-2 cell growth, the medium was removed from filter wells and from the receiver plate, which were filled with fresh HBSS buffer (Invitrogen). This procedure was repeated twice, and the plates were incubated at 37 °C for 30 min. After incubation time, the HBSS buffer was removed and drug solutions and reference compounds, were added to the filter well at the concentration of 100 μM, while fresh HBSS was added to the receiver plate. The plates were incubated at 37 °C for 120 min. Afterwards, samples

were removed from the apical (filter well) and basolateral (receiver plate) side of the monolayer to measure the permeability.

The apparent permeability (Papp), in units of nm/second, was calculated using the following equation:

$$P_{app} = \left(\frac{V_A}{\text{Area} \times \text{time}} \right) \times \left(\frac{[\text{drug}]_{\text{acceptor}}}{[\text{drug}]_{\text{initial}}} \right)$$

VA = the volume (in mL) in the acceptor well;

Area = the surface area of the membrane (0.11 cm^2 of the well);

time = the total transport time in seconds (7200 sec);

[drug]acceptor = the concentration of the drug measured by U.V. spectroscopy;

[drug]initial = the initial drug concentration (1 × 10-4 M) in the apical or basolateral wells.

Antiproliferative assay. Determination of cell growth was performed using the MTT assay at 48 h and 72 h.[33] On day 1, 10000 cells/well were seeded into 96-well plates in a volume of 100 μL. On day 2, the drugs concentration (0.1, 1, 10, 25 μM) were added. In all the experiments, the various drug-solvents (ethanol, DMSO) were added in each control to evaluate a possible solvent cytotoxicity. After the established incubation time with drugs, MTT (0.5 mg/mL) was added to each well, and after 3 h incubation at 37°C, the supernatant was removed. The formazan crystals were solubilized using 100 μL of DMSO and the absorbance values at 570 and 630 nm were determined on the microplate reader Victor 3 from PerkinElmer Life Sciences.

Co-administration Assay. The co-administration assay with Doxorubicin was performed in MDCK-MDR1 cells at 48h as reported with minor modification.[34] On day 1, 10000 cells/well were seeded into 96-well plates in a volume of 100 μL of fresh medium. On day 2, the tested drug was added alone to the cells at different concentrations (10 nM, 100 nM, 1 μM). On day 3, the medium was removed and the drug at the same concentrations was added alone and in co-administration with 10 μM Doxorubicin to the cells. After the established incubation time with the tested drug, MTT (0.5 mg/mL) was added to each well, and after 3-4 h incubation at 37 °C, the supernatant was removed. The formazan crystals were solubilized using 100 μL of DMSO/EtOH (1:1), and the absorbance values at 570 and 630 nm were determined on the microplate reader Victor 3 from PerkinElmer Life Sciences.

Cancer stem cells isolation and characterization. For GB, samples collected during surgical resection of glioblastoma, were obtained from the Neuro-Bio-Oncology Center, Vercelli, Italy and cultured as DC or SC as previously described,[35] with minor modifications.[36] For DC, DMEM supplemented with 1 % PS, 10% v/v FBS was used. For SC, DMEM-F12 medium was supplemented with 1 M HEPES, 0.3 mg/mL glucose, 75 μg/mL $NaHCO_3$, 2 mg/mL heparin, 2 mg/mL bovine serum albumin, 2 mM progesterone, 20 ng/mL EGF, 10 ng/mL bFGF. DC were obtained from dissociated SC, centrifuged at 1,200 × g for 5 min and seeded in DC medium. *In vitro* clonogenicity and self-renewal, *in vivo* tumourigenicity were reported in ref. 10.[10] The percentage of cells positive for general stemness markers was further quantified by flow cytometry. Cells were washed with PBS, detached with Cell Dissociation Solution (Sigma Chemical Co.), re-suspended in culture medium containing 5 μL/100 mL FBS, incubated with antibodies recognizing CD133 (Miltenyi Biotec, Bergisch Gladbach, Germany), Musashi-1 (Millipore, Billerica, MA), SOX2 (Biolegend, San Diego, CA), Oct4 (Cell Signaling

Technology, Danvers, MA), Nanog (Cell Signaling Technology,), and ABCG2 (Santa Cruz Biotechnology Inc., Santa Cruz, CA), followed by the secondary fluorescein isothiocyanate (FITC)-conjugated antibody (30 min at 4 ^{o}C) and fixation in 25 µg/mL paraformaldehyde. Aldehyde dehydrogenase-Based Cell Detection Kit (Stemcell Technologies, Vancouver, Canada) was used to calculate the percentage of Aldehyde dehydrogenase (ALDH)^{bright} cells, 5×10^5 cells were analyzed by the Guava® *easyCyte* flow cytometer, using the InCyte software (Millipore). Control experiments included incubation of cells with non-immune isotypic antibody, followed by secondary antibody.

MPM cells were obtained from thoracoscopies of patients with pathological diagnosis of mesothelioma. Tissue was digested in medium containing 1 mg/ml collagenase and 0.2 mg/mL hyaluronidase for 1 h at 37°C. From each sample DC and SC were obtained. DC were cultured in HAM F12 medium supplemented with % PS and 10% FBS. SC were generated from DC by maintaining them in HAM F12/DMEM medium supplemented 1% PS, 20 ng/mL EGF, 20 ng/mL b-FGF, 4 µg/mL IGF-1, 0.2% B27 (Invitrogen, Milano, Italy), replaced twice a week. After two weeks in these culture conditions, SC were isolated by cell sorting of SOX2$^+$ Oct4$^+$ Nanog$^+$ ABCG2$^+$ ALDH^{bright} cells, using the same antibodies and kits listed above.

Patients were anonymized and referred to as patient #1,#2,#3. Cells were seeded in culture and used within passage 6. The Ethical Committee of the Hosting Institution, University of Torino, approved the study (#ORTO11WNST; #126/2016).

Intracellular Doxorubicin accumulation. Cells were incubated 3 h with 5 µM doxorubicin, washed with PBS, trypsinized, centrifuged at 13,000 × g for 5 min and re-suspended in 0.5 mL of 1/1 solution ethanol/0.3 N HCl. A 50 µL aliquot was sonicated and used for the measurement of the protein content. The intracellular fluorescence of doxorubicin was measured

spectrofluorimetrically, using a Synergy HT microplate Reader (Bio-Tek Instruments, Winooski, VT). Excitation and emission wavelengths were 475 nm and 553 nm. Fluorescence was converted in nmol/mg cell proteins, using a calibration curve previously set.

Primary cell viability. DC and SC viability was measured by the ATPlite Luminescence Assay System (PerkinElmer, Waltham, MA), as per manufacturer's instructions, using a Synergy HT Multi-Detection Microplate Reader. The relative luminescence units (RLU) of untreated cells were considered as 100% viability; results were expressed as a percentage of viable cells versus untreated cells.

Statistical analysis. All data in the text and figures are provided as means ± SEM. The results were analysed by a Student's t-test and ANOVA test, using Graph-Pad Prism (Graph-Pad software, San Diego, CA, USA). $p < 0.05$ was considered significant.

ASSOCIATED CONTENT

Supporting Information. The following files are available free of charge. Experimental procedures for: synthesis of compounds, PCR array, immunoblotting, lactate dehydrogenase (LDH) release, P-gp knock-out and ionization constant measurement. Molecular modelling details (PDF). Molecular Formula String file for target compounds (csv). PDB coordinate files for complexes including **5b** and **6** used for dynamic analysis (PDB).

AUTHOR INFORMATION

Corresponding Author

*SG: stefano.guglielmo@unito.it

*MC: marialessandra.contino@uniba.it

Author Contributions

The manuscript was written through contributions of all authors. All authors have given approval to the final version of the manuscript.

ACKNOWLEDGMENT

This study was supported by the University of Turin – "Ricerca Locale" (grant GUGS_RILO_17_01 to SG), by MIUR (grant GUGS_FFABR_17_01 to SG, FIRB 2012 RBFR12SOQ1_002, FIRB 2012, grant RBFR12SOQ1 to CR; FABR grant to MAC, CR), by My First AIRC Grant-MFAG2015 (Project Id.17566 to MGP) and AIRC-IG2014 (IG15232 to CR). SG was granted with access to computational facilities at Occam supercomputer,[37] Scientific Computing Competence Centre (C3S) of the University of Turin and with resources at CINECA (ISCRA HP10CL3AHF to SG). We are thankful to Prof. A. Gasco for fruitful discussion.

ABBREVIATIONS

CSCs, Cancer stem cells; ABC, ATP Binding Cassette; NBD, nucleotide-binding domains; TMD, two transmembrane domains; BCRP Breast Cancer Resistance Protein; P-gp, P-glycoprotein; MDR Multi Drug Resistance; P_{app}, Apparent Permeability; GB, glioblastoma; MPM, malignant pleural mesothelioma; TLC, thin layer chromatography.

REFERENCES

(1) Begicevic, R.-R.; Falasca, M. ABC Transporters in Cancer Stem Cells: Beyond Chemoresistance. *Int. J. Mol. Sci.* **2017**, *18* (11), 2362.

(2) Zinzi, L.; Contino, M.; Cantore, M.; Capparelli, E.; Leopoldo, M.; Colabufo, N. A. ABC Transporters in CSCs Membranes as a Novel Target for Treating Tumor Relapse. *Front. Pharmacol.* **2014**, *5 JUL* (July), 1–13.

(3) Beier, D.; Schulz, J. B.; Beier, C. P. Chemoresistance of Glioblastoma Cancer Stem Cells - Much More Complex than Expected. *Mol. Cancer* **2011**, *10*, 1–11.

(4) Ren, F.; Shen, J.; Shi, H.; Hornicek, F. J.; Kan, Q.; Duan, Z. Novel Mechanisms and Approaches to Overcome Multidrug Resistance in the Treatment of Ovarian Cancer. *Biochim. Biophys. Acta - Rev. Cancer* **2016**, *1866* (2), 266–275.

(5) Ryoo, I. G.; Kim, G.; Choi, B. H.; Lee, S. H.; Kwak, M. K. Involvement of NRF2 Signaling in Doxorubicin Resistance of Cancer Stem Cell-Enriched Colonospheres. *Biomol. Ther.* **2016**, *24* (5), 482–488.

(6) Moreira, H.; Szyjka, A.; Gąsiorowski, K. Chemopreventive Activity of Celastrol in Drug-Resistant Human Colon Carcinoma Cell Cultures. *Oncotarget* **2018**, *9* (30), 21211–21223.

(7) Mimeault, M.; Batra, S. K. Recent Progress on Tissue-Resident Adult Stem Cell Biology and Their Therapeutic Implications. *Stem Cell Rev.* **2008**, *4* (1), 27–49.

(8) Alexandra E. Stacy, P. J. J. and D. R. R. Molecular Pharmacology of ABCG2 and Its Role in Chemoresistance. *Mol. Pharmacol.* **2013**, *84* (5), 655–669.

(9) Gottesman, M. M.; Fojo, T.; Bates, S. E. Multidrug Resistance in Cancer: Role of Atp-Dependent Transporters. *Nat. Rev. Cancer* **2002**, *2* (1), 48–58.

(10) Riganti, C.; Salaroglio, I. C.; Caldera, V.; Campia, I.; Kopecka, J.; Mellai, M.; Annovazzi, L.; Bosia, A.; Ghigo, D.; Schiffer, D. Temozolomide Downregulates P-Glycoprotein Expression in Glioblastoma Stem Cells by Interfering with the Wnt3a / Glycogen Synthase-3 Kinase / b -Catenin Pathway. *Neuro. Oncol.* **2013**, *15* (11), 1502–1517.

(11) Sandoval, T. A.; Urueña, C. P.; Llano, M.; Gómez-Cadena, A.; Hernández, J. F.; Sequeda, L. G.; Loaiza, A. E.; Barreto, A.; Li, S.; Fiorentino, S. Standardized Extract from *Caesalpinia Spinosa* Is Cytotoxic Over Cancer Stem Cells and Enhance Anticancer Activity of Doxorubicin. *Am. J. Chin. Med.* **2016**, *44* (08), 1693–1717.

(12) Wagner-Souza, K.; Diamond, H. R.; Ornellas, M. H.; Gomes, B. E.; Almeida-Oliveira, A.; Abdelhay, E.; Bouzas, L. F.; Rumjanek, V. M. Rhodamine 123 Efflux in Human Subpopulations of Hematopoietic Stem Cells: Comparison between Bone Marrow, Umbilical Cord Blood and Mobilized Peripheral Blood CD34+ Cells. *Int J Mol Med* **2008**, *22* (2), 237–242.

(13) Linn, D. E.; Yang, X.; Sun, F.; Xie, Y.; Chen, H.; Jiang, R.; Chen, H.; Chumsri, S.; Burger, A. M.; Qiu, Y. A Role for OCT4 in Tumor Initiation of Drug-Resistant Prostate Cancer Cells. *Genes and Cancer* **2010**, *1* (9), 908–916.

(14) Colabufo, N. A.; Berardi, F.; Cantore, M.; Perrone, M. G.; Contino, M.; Inglese, C.; Niso, M.; Perrone, R.; Azzariti, A.; Simone, G. M.; Porcelli, L.; Paradiso, A. Small P-Gp Modulating Molecules: SAR Studies on Tetrahydroisoquinoline Derivatives. *Bioorganic*

Med. Chem. **2008**, *16* (1), 362–373.

(15) Colabufo, N. A.; Berardi, F.; Perrone, M. G.; Cantore, M.; Contino, M.; Inglese, C.; Niso, M.; Perrone, R. Multi-Drug-Resistance-Reverting Agents: 2-Aryloxazole and 2-Arylthiazole Derivatives as Potent BCRP or MRP1 Inhibitors. *ChemMedChem* **2009**, *4* (2), 188–195.

(16) Guglielmo, S.; Contino, M.; Lazzarato, L.; Perrone, M. G.; Blangetti, M.; Fruttero, R.; Colabufo, N. A. A Potent and Selective P-Gp Modulator for Altering Multidrug Resistance Due to Pump Overexpression. *ChemMedChem* **2016**, *11* (4).

(17) Guglielmo, S.; Lazzarato, L.; Contino, M.; Perrone, M. G.; Chegaev, K.; Carrieri, A.; Fruttero, R.; Colabufo, N. A.; Gasco, A. Structure-Activity Relationship Studies on Tetrahydroisoquinoline Derivatives: [4′-(6,7-Dimethoxy-3,4-Dihydro-1H-Isoquinolin-2-Ylmethyl)Biphenyl-4-Ol] (MC70) Conjugated through Flexible Alkyl Chains with Furazan Moieties Gives Rise to Potent and Selective. *J. Med. Chem.* **2016**, *59* (14).

(18) Contino, M.; Guglielmo, S.; Perrone, M. G.; Giampietro, R.; Rolando, B.; Carrieri, A.; Zaccaria, D.; Chegaev, K.; Borio, V.; Riganti, C.; Zabielska-Koczywąs, K.; Colabufo, N. A.; Fruttero, R. New Tetrahydroisoquinoline-Based P-Glycoprotein Modulators: Decoration of the Biphenyl Core Gives Selective Ligands. *Medchemcomm* **2018**, *9* (5), 862–869.

(19) Meanwell, N. A. Synopsis of Some Recent Tactical Application of Bioisosteres in Drug Design. *J. Med. Chem.* **2011**, *54* (8), 2529–2591.

(20) Esser, L.; Zhou, F.; Pluchino, K. M.; Shiloach, J.; Ma, J.; Tang, W. K.; Gutierrez, C.; Zhang, A.; Shukla, S.; Madigan, J. P.; Zhou, T.; Kwong, P. D.; Ambudkar, S. V.; Gottesman, M. M.; Xia, D. Structures of the Multidrug Transporter P-Glycoprotein Reveal

Asymmetric ATP Binding and the Mechanism of Polyspecificity. *J. Biol. Chem.* **2017**, *292* (2), 446–461.

(21) Liu, C.; Zhang, Y.; Liu, N.; Qiu, J. A Simple and Efficient Approach for the Palladium-Catalyzed Ligand-Free Suzuki Reaction in Water. *Green Chem.* **2012**, *14* (11), 2999–3003.

(22) Li, M.; Lincoln, P. Synthesis and DNA Threading Properties of Quaternary Ammonium [Ru(Phen)2(Dppz)]2+derivatives. *J. Inorg. Biochem.* **2009**, *103* (7), 963–970.

(23) Crawford, J. J.; Lee, W.; Aliagas, I.; Mathieu, S.; Hoeflich, K. P.; Zhou, W.; Wang, W.; Rouge, L.; Murray, L.; La, H.; Liu, N.; Fan, P. W.; Cheong, J.; Heise, C. E.; Ramaswamy, S.; Mintzer, R.; Liu, Y.; Chao, Q.; Rudolph, J. Structure-Guided Design of Group I Selective P21-Activated Kinase Inhibitors. *J. Med. Chem.* **2015**, *58* (12), 5121–5136.

(24) Kajita, H.; Togni, A. A Oxidative Bromination of (Hetero)Arenes in the TMSBr/DMSO System: A Non-Aqueous Procedure Facilitates Synthetic Strategies. *ChemistrySelect* **2017**, *2* (3), 1117–1121.

(25) Capparelli, E.; Zinzi, L.; Cantore, M.; Contino, M.; Perrone, M. G.; Luurtsema, G.; Berardi, F.; Perrone, R.; Colabufo, N. A. SAR Studies on Tetrahydroisoquinoline Derivatives: The Role of Flexibility and Bioisosterism to Raise Potency and Selectivity toward P-Glycoprotein. *J. Med. Chem.* **2014**, *57* (23), 9983–9994.

(26) Cortes-Dericks, L.; Froment, L.; Boesch, R.; Schmid, R. A.; Karoubi, G. Cisplatin-Resistant Cells in Malignant Pleural Mesothelioma Cell Lines Show ALDHhighCD44+ Phenotype and Sphere-Forming Capacity. *BMC Cancer* **2014**, *14* (1), 304.

(27) Callaghan, R.; Luk, F.; Bebawy, M. Inhibition of the Multidrug Resistance P-Glycoprotein: Time for a Change of Strategy? *Drug Metab. Dispos.* **2014**, *42* (4), 623–

631.

(28) Barducci, A.; Bussi, G.; Parrinello, M. Well-Tempered Metadynamics: A Smoothly Converging and Tunable Free-Energy Method. *Phys. Rev. Lett.* **2008**, *100* (2), 020603.

(29) Tiwary, P.; Parrinello, M. From Metadynamics to Dynamics. *Phys. Rev. Lett.* **2013**, *111* (23).

(30) Bakan, A.; Meireles, L. M.; Bahar, I. ProDy: Protein Dynamics Inferred from Theory and Experiments. *Bioinformatics* **2011**, *27*, 1575–1577.

(31) Ferreira, R. J.; Ferreira, M. J. U.; Dos Santos, D. J. V. A. Insights on P-Glycoproteins Efflux Mechanism Obtained by Molecular Dynamics Simulations. *J. Chem. Theory Comput.* **2012**, *8*, 1853–1864.

(32) Callaghan, R.; Ford, R. C.; Kerr, I. D. The Translocation Mechanism of P-Glycoprotein. *FEBS Letters*. 2006, pp 1056–1063.

(33) Colabufo, N. A.; Contino, M.; Cantore, M.; Capparelli, E.; Perrone, M. G.; Cassano, G.; Gasparre, G.; Leopoldo, M.; Berardi, F.; Perrone, R. Naphthalenyl Derivatives for Hitting P-Gp/MRP1/BCRP Transporters. *Bioorganic Med. Chem.* **2013**, *21* (5), 1324–1332.

(34) Tardia, P.; Stefanachi, A.; Niso, M.; Stolfa, D. A.; Mangiatordi, G. F.; Alberga, D.; Nicolotti, O.; Lattanzi, G.; Carotti, A.; Leonetti, F.; Perrone, R.; Berardi, F.; Azzariti, A.; Colabufo, N. A.; Cellamare, S. Trimethoxybenzanilide-Based P-Glycoprotein Modulators: An Interesting Case of Lipophilicity Tuning by Intramolecular Hydrogen Bonding. *J. Med. Chem.* **2014**, *57* (15), 6403–6418.

(35) Reynolds, B. A.; Tetzlaff, W.; Weiss, S. A Multipotent EGF-Responsive Striatal Embryonic Progenitor Cell Produces Neurons and Astrocytes. *J. Neurosci.* **1992**, *12* (11), 4565–4574.

(36) Caldera, V.; Mellai, M.; Annovazzi, L.; Piazzi, A.; Lanotte, M.; Cassoni, P.; SChiffer, D. Antigenic and Genotypic Similarity between Primary Glioblastomas and Their Derived Neurospheres. *J. Oncol.* **2011**, *2011*, 314962.

(37) Aldinucci, M.; Bagnasco, S.; Lusso, S.; Pasteris, P.; Rabellino, S.; Vallero, S. OCCAM: A Flexible, Multi-Purpose and Extendable HPC Cluster. *J. Phys. Conf. Ser.* **2017**, *898*, 082039.

Table of Contents Graphics